International Journal of Solids and Structures 45 (2008) 5483–5501

Contents lists available at ScienceDirect

International Journal of Solids and Structures

journal homepage: www.elsevier.com/locate/ijsolstr

Development of an approach to constitutive modelling of concrete: Isotropic damage coupled with plasticity

Giang D. Nguyen [a,*], Alexander M. Korsunsky [b]

[a] Department of Mathematics and Statistics, University of New Mexico, Albuquerque, NM 87131, USA
[b] Department of Engineering Science, University of Oxford, Parks Road, Oxford OX1 3PJ, UK

ARTICLE INFO

Article history:
Received 25 March 2007
Received in revised form 6 July 2007
Available online 7 June 2008

Keywords:
Constitutive modelling
Concrete
Damage
Plasticity
Parameter identification

ABSTRACT

The paper presents an approach to constitutive modelling of concrete using damage mechanics and plasticity theory. The thermodynamic formulation, and parameter identification of a non-local coupled damage-plasticity model are presented in this study. The particular focus is the calibration of model parameters. It is shown that both the local parameters and the parameters governing the non-local interaction can be determined from experimental data reliably and consistently. A novel procedure is developed for parameter identification, using the separation of total dissipation energy into additive parts corresponding to different dissipation mechanisms. The relationship between the local and non-local parameters is also addressed, helping to obtain model responses consistent with the fracture energy of the material. The application of the model and the calibration procedure proposed in this study to the numerical failure analysis of concrete structures is illustrated through a series of real structural tests, showing both the performance of the model and the consistency of the proposed calibration procedure.

1. Introduction

In constitutive modelling of concrete, the use of coupling between damage and plasticity has been found to be essential for capturing the observed phenomenological behaviour of the material. Coupled damage-plasticity models for concrete have been developed and used by several researchers, e.g. Simo and Ju (1987a,b), Yazdani and Schreyer (1988), Luccioni et al. (1996), Lee and Fenves (1998a,b), Meschke et al. (1998), Hansen et al. (2001), Addessi et al. (2002), Jefferson (2003a,b), Salari et al. (2004). On the other hand, non-local regularization techniques (Pijaudier-Cabot and Bazant, 1987) have been widely used in the modelling of softening materials, and help to avoid pathological problems encountered in the constitutive modelling of these materials (e.g. Jirásek, 1998; Ferrara and Di Prisco, 2001; Comi, 2001; Addessi et al., 2002). Nevertheless, not many of the existing non-local coupled damage-plasticity models have been constructed on the basis of a consistent approach which encompasses a thermodynamic formulation, an enhancement to the constitutive models to deal with softening-related problems, and a consistent procedure for the parameter identification and determination. This, to the authors' point of view, obviously restricts the applicability and the reliability of these models in practice.

The identification and determination of the model parameters plays an important role in the development of constitutive models, especially non-local models in which two sets of model parameters control (a) the local behaviour of the non-local model and (b) the spatial interaction of material points. The local set of parameters in this case is related to the behaviour of the model at a pointwise level. On the other hand, the spatial parameter governing the interaction of material points is the

* Corresponding author. Present address: School of Civil Engineering, J05, The University of Sydney, Sydney, NSW 2006, Australia. Tel.: +61 2 9351 3721; fax: +61 2 9351 3343.
E-mail addresses: giang.nguyen@trinity.oxon.org, giang.nguyen@usyd.edu.au (G.D. Nguyen), alexander.korsunsky@eng.ox.ac.uk (A.M. Korsunsky).

0020-7683/$ - see front matter © 2008 Elsevier Ltd. All rights reserved.
doi:10.1016/j.ijsolstr.2008.05.029

length parameter l, which is also termed the internal length (or characteristic length) of the non-local continuum and is related to the width of the damage zone. These two sets of parameters are closely related to each other and should be appropriately determined to give the non-local model a response consistent with the required macroscopic material properties. The appearance of the spatial parameter here requires the solution of boundary value problems for the determination of model parameters. This is totally different from a local approach, where the (pointwise) constitutive behaviour of the model can be calibrated directly from experimental data, without the need for solutions of boundary value problems (Nguyen and Houlsby, 2007).

For local coupled damage-plasticity behaviour, the calibration of model parameters so far has been rarely addressed in detail (e.g. in Meschke et al., 1998; Jefferson, 2003b). The choice of model parameters sometimes appears to be rather arbitrary (e.g. in Luccioni et al., 1996), without a clear connection with the experimental methods used to determine the mechanical properties of the material. From experimental point of view, Bazant (1996) showed that the fracture energy G_F determined by the work-of-fracture method always contains plastic-frictional energy dissipation (e.g. due to aggregate interlocking, frictional slips or pull-out of fragments). This conclusion is substantiated by cyclic tests on the tensile-dominant behaviour of concrete (Reinhardt et al., 1986; Perdikaris and Romeo, 1995). As a consequence, in constitutive modelling the fracture energy G_F should be thought of containing contributions from both failure mechanisms, damage and plasticity. However, the fact that G_F does not reflect purely the damage fracture energy has been disregarded in many damage-based models for concrete. In addition, the experimental evidence on the separation of total dissipated energy in concrete fracture seems not to have been used for parameter calibration in the literature.

On the other hand, the existing approaches to calibration of parameters of non-local models based on inverse analysis (Carmeliet, 1999; Mahnken and Kuhl, 2003; Le Bellego et al., 2003) appear too complicated and computationally costly to apply widely in practice. Besides, other simple types of calibration based on a linear relationship between the length parameter l and the actual width of the localization zone (De Borst and Muhlhaus, 1992; De Borst and Pamin, 1996; Meftah and Reynouard, 1998; Di Prisco et al., 2000) cannot be considered versatile enough to be applicable for different non-local models with different softening laws and different types of non-local averaging (e.g. non-locality of damage energy, damage variable or strain using Gauss distribution function or other bell-shaped functions).

The motivation of this study is to develop a consistent approach using damage mechanics and plasticity theory for the numerical simulation of concrete structures. At this early stage, only 2D plane stress behaviour of concrete in tensile regime is considered. The thermodynamic formulation, non-local regularization and the parameter identification form interrelating parts of the development of a coupled damage-plasticity model. However the particular focus of this study is placed on the parameter identification. The model presented in this study is an initial attempt to model important features of the material behaviour within a consistent and rigorous approach. Generalization of the behaviour of a single crack in mode I opening, simulated here through an isotropic damage-plasticity model, is only briefly described and expected to progress further in future work. Earlier works (e.g. Markeset and Hillerborg, 1995; Schreyer, 2007) could be used as a guide to enhance the constitutive behaviour of the model proposed in this study.

The paper is organized as follows. A coupled damage-plasticity model based on a thermodynamic formulation is presented in Section 2. Improvement over models in Nguyen (2005), and Nguyen and Houlsby (2008a) is also suggested and described through the incorporation of anisotropic features. With our main aim of illustrating the consistency of the formulation and the calibration procedure for model parameters, this improvement is however not yet incorporated in the implementation. Instead a simpler isotropic version of the proposed anisotropic model is used throughout the study. This helps to simplify the algorithm. The introduction of non-local behaviour into the model is also briefly described. In Section 3, the calibration of parameters governing the non-local behaviour of the model is presented. Local parameters governing the damage and yielding processes are calibrated based on the damage dissipation energy and plastic-frictional dissipation energy, respectively. All model parameters are shown to be identifiable and consistently determined from the experimentally measured properties of the material. On the other hand, the link between local and spatial sets of parameters governing the behaviour of the non-local coupled damage-plasticity model is also considered. This is to obtain model responses consistent with the experimentally measured fracture properties of the material. Numerical examples are presented in Section 4 to demonstrate the capability of non-local model and the advantageous features of the proposed calibration procedures.

2. Local models based on thermodynamics

2.1. Formulation

This section briefly presents a simple formulation for a class of continuum elasto-plastic-damageable models based on the thermodynamic framework developed by Houlsby and Puzrin (2000) and modified somewhat by Nguyen (2005). Details of the formulation can be found in Nguyen (2005) and Nguyen and Houlsby (2008a). For the sake of simplicity a Drucker-Prager type yield criterion is adopted and its derivation incorporated in the formulation. This yield criterion in this case is coupled with a damage criterion, which is based on the damage energy release rate. Use of this simple yield criterion is obviously not a very good choice (e.g. no difference between tensile, shear and compressive meridians; linear relationship between normal and shear stresses in the meridian plane) but sufficient for our purpose of illustration of the calibration procedure in the next sections.

The energy and dissipation potentials are assumed to have the following forms:

$$g = -\frac{D_{ijkl}\sigma_{ij}\sigma_{kl}}{2(1-\alpha_d)} - \sigma_{ij}\alpha_{ij} \tag{1}$$

$$d = d_d + d_p + \Lambda_1 C_1 + \Lambda_2 C_2 = F_1^*(\alpha_d, \sigma_{ij})\dot{\alpha}_d + k\sqrt{2\dot{\alpha}'_{ij}\dot{\alpha}'_{ij}} + \Lambda_1 C_1 + \Lambda_2 C_2 \tag{2}$$

in which α_{ij} and α_d are the plastic strain tensor and the scalar damage variable, respectively; D_{ijkl} is the elasticity compliance tensor expressed for the isotropic case in terms of Young's modulus E and Poisson's ratio v as

$$D_{ijkl} = \frac{1+v}{2E}\left(-\frac{2v}{1+v}\delta_{ij}\delta_{kl} + \delta_{ik}\delta_{jl} + \delta_{il}\delta_{jk}\right)$$

d_d and d_p are the dissipation contributions due to damage and plasticity, respectively; and

$$C_1 = \dot{\alpha}_{kk}/3 - \beta\sqrt{2\dot{\alpha}'_{ij}\dot{\alpha}'_{ij}} = 0 \tag{3}$$

$$C_2 = \dot{\varepsilon}_p - c\sqrt{\dot{\alpha}_{ij}\dot{\alpha}_{ij}} = \dot{\varepsilon}_p - \sqrt{2\dot{\alpha}_{ij}\dot{\alpha}_{ij}/3} = 0 \tag{4}$$

are two constraints used to define a pressure-dependent yield criterion and the accumulated plastic strain ε_p, respectively. The Lagrangian multipliers Λ_1 and Λ_2 in (2) are associated with these two constraints (see Houlsby and Puzrin (2000)). In the dissipation function (2), $F_1^*(\alpha_d, \sigma_{ij})$ is a positive and monotonically increasing scalar function associated with the damage process. The two parameters k and β in (3) and (4) are defined as functions of the yield stresses f_{ty} and f_{cy} in tension and compression, respectively:

$$\beta = \frac{f_{cy} - f_{ty}}{\sqrt{3}(f_{cy} + f_{ty})} \text{ and } k = \frac{2f_{cy}f_{ty}}{\sqrt{3}(f_{cy} + f_{ty})} \tag{5}$$

For simplicity, linear hardening is assumed here, and damage variable is introduced into the expressions of f_{ty} and f_{cy} so that these yield stresses reduce with progressive damage. Therefore we have

$$f_{cy} = (1-\alpha_d)(f'_c + H_t\varepsilon_p) \tag{6}$$

$$f_{ty} = (1-\alpha_d)(f'_t + H_t\varepsilon_p) \tag{7}$$

with $H_t > 0$ denoting the hardening modulus, and f'_c and f'_t being the ultimate stresses in uniaxial compression and tension, respectively.

The derivation of the constitutive models here follows standard procedures established in the original framework (Houlsby and Puzrin, 2000), and illustrated in Nguyen (2005) and Nguyen and Houlsby (2008a). Therefore it is not necessary to repeat the details here. We can write the derived constitutive equations as follows:

$$\varepsilon_{ij} = \frac{D_{ijkl}\sigma_{kl}}{1-\alpha_d} + \alpha_{ij} \tag{8}$$

$$y_p = \beta\sigma_{kk} + \sqrt{\frac{\sigma'_{ij}\sigma'_{ij}}{2}} - k = 0 \tag{9}$$

$$y_d = \frac{D_{ijkl}\sigma_{ij}\sigma_{kl}}{2(1-\alpha_d)^2} - F_1^*(\alpha_d, \sigma_{ij}) = 0 \tag{10}$$

In the damage criterion (10), the choice of function $F_1^*(\alpha_d, \sigma_{ij})$ is flexible, provided that it is non-negative to assure the thermodynamic admissibility of the dissipation process. Here the following form of $F_1^*(\alpha_d, \sigma_{ij})$ is adopted:

$$F_1^*(\alpha_d, \sigma_{ij}) = \begin{cases} 0 & \text{if } \sigma_{ij} = 0 (i,j = 1\cdots 3) \\ \left[\dfrac{D_{ijkl}\sigma_{ij}\sigma_{kl}}{2(1-\alpha_d)^2}\right]\dfrac{F_1(\alpha_d)}{F_2(\sigma_{ij})} & \text{otherwise} \end{cases} \tag{11}$$

where $F_1(\alpha_d)$ and $F_2(\sigma_{ij})$ are two scalar-valued and positive functions, the forms of which govern the damage evolution law and the shape of damage surface, respectively. Substitution of (11) into (10) leads to

$$y_d = \left[\frac{D_{ijkl}\sigma_{ij}\sigma_{kl}}{2(1-\alpha_d)^2}\right]\left[1 - \frac{F_1(\alpha_d)}{F_2(\sigma_{ij})}\right] = 0 \tag{12}$$

Since the first bracketed term in (12) is an energy-like term which is positive definite in non-zero stress states, its elimination in (12) is straightforward. Therefore, the damage function y_d can be rewritten in a simplified form as

$$y_d = F_2(\sigma_{ij}) - F_1(\alpha_d) = 0 \tag{13}$$

The choices of $F_2(\sigma_{ij})$ and $F_1(\alpha_d)$ are flexible here to obtain the desired shape of the damage surface and damage evolution law. In the model used here, we choose

$$F_2(\sigma_{ij}) = \frac{(1+p_t)\sigma_{ij}^+\sigma_{ij}^+ - p_t\langle\sigma_{kk}\rangle\langle\sigma_{ll}\rangle}{2E(1-\alpha_d)^2} \tag{14}$$

and

$$F_1(\alpha_d) = \frac{f_t'^2}{2E}\left[\frac{E + E_{pt}(1-\alpha_d)^{n_t}}{E(1-\alpha_d) + E_{pt}(1-\alpha_d)^{n_t}}\right]^2 \tag{15}$$

in which p_t is a parameter controlling the shape of the damage surface in stress space; E_{pt} and n_t are two parameters governing the damage evolution, the physical interpretations and calibration of which will be detailed in Section 3.1. In (14), σ_{ij}^+ denotes the positive part of the total stress tensor σ_{ij}, which is decomposed into positive and negative parts using the eigenvalue decomposition (Ladeveze, 1983; Ortiz, 1985):

$$\sigma_{ij}^+ = \sum_{m=1}^{3}\langle\sigma^m\rangle p_i^m p_j^m$$

where $\mathbf{p}^m$ is the unit vector of the mth principal direction and σ^m is the mth principal stress. Further details and some properties of the decomposition can be found in Ladeveze (1983) and Ortiz (1985).

2.2. Extension to cases with anisotropy

The model described above is just a simple isotropic model to be used as a means to illustrate some features of the approach, particularly the calibration of model parameters. Although it can capture the behaviour of concrete in some real tests, e.g. bending and tension tests, its capability is limited, as discussed in Nguyen (2005) and Nguyen and Houlsby (2008a). Modifications are proposed here, although not implemented yet, to take into account the anisotropic features of the material behaviour. Despite the use of tensorial damage variable in the literature (Ladeveze, 1983; Ju, 1990; Murakami and Kamiya, 1997), in our opinion scalar form of damage variable still remains attractive for a number of reasons. This is thanks to its simplicity in the formulation, implementation and calibration of model parameters, the last of which is particularly addressed in this study. The capability of the model in capturing the anisotropic features of the material behaviour is however not restricted by the use of damage as scalar variables.

Modifications are made here to the formulation described in the preceding section. The Gibbs free energy function can be modified as follows:

$$g = -\frac{D_{ijkl}\sigma_{ij}^*\sigma_{kl}^*}{2(1-\alpha_d)} - \frac{D_{ijkl}\sigma_{ij}^{**}\sigma_{kl}^{**}}{2} - D_{ijkl}\sigma_{ij}^*\sigma_{kl}^{**} - \sigma_{ij}\alpha_{ij} \tag{16}$$

It is noted here that (16) is now written in the local coordinate system **n**–**t**–**p** associated with the orientation of a crack (Fig. 1). In the absence of damage and plasticity, the above function reduces to the usual form of the elastic Gibbs free energy potential, thus fulfilling basic thermodynamic requirements. The total stress tensor σ_{ij} in (16) is assumed to be decomposed into two additive parts, σ_{ij}^* and σ_{ij}^{**}, defined in the local coordinate system **n**–**t**–**p** by

$$\sigma_{ij}^* = \begin{bmatrix} \sigma_{nn} & \tau_{nt} & \tau_{pn} \\ \tau_{nt} & 0 & 0 \\ \tau_{pn} & 0 & 0 \end{bmatrix} \text{ and } \sigma_{ij}^{**} = \begin{bmatrix} 0 & 0 & 0 \\ 0 & \sigma_{tt} & \tau_{tp} \\ 0 & \tau_{tp} & \sigma_{pp} \end{bmatrix} \tag{17}$$

The strain in the local coordinate system **n**–**t**–**p** is now

$$\varepsilon_{ij} = -\frac{\partial g}{\partial\sigma_{ij}} = D_{mnkl}\frac{\partial\sigma_{mn}^*}{\partial\sigma_{ij}}\left[\frac{\sigma_{kl}^*}{(1-\alpha_d)} + \sigma_{kl}^{**}\right] + D_{mnkl}\sigma_{kl}\frac{\partial\sigma_{mn}^{**}}{\partial\sigma_{ij}} + \alpha_{ij} \tag{18}$$

As can be seen, only certain components of the total stress tensor, such as tractions on the crack surface, are directly affected by damage. These tractions should vanish once full separation of two crack surfaces occurs, characterized by damage α_d

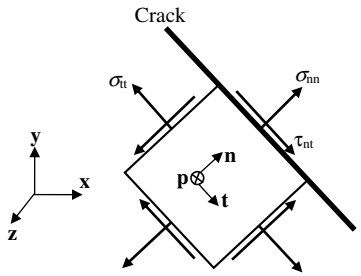

Fig. 1. Local coordinate system **n**–**t**–**p** associated with a crack.

reaching unity in the model here. In addition, for a given direction, the derivatives of the stresses σ_{ij}^{*} and σ_{ij}^{**} with respect to total stress tensor σ_{ij} are fourth order tensors of constant values. Therefore they do not complicate the numerical implementation. Further extension of the formulation to cases with multiple intersecting cracks at the same material point is feasible in principle, with the use of multiple scalar damage variables. Nevertheless, the above modifications are only described in general form and therefore full features of the model (e.g. capability to avoid stress locking when the crack is widely opened, the behaviour in fracture mode II as well as in the transition between modes I and II) should be further investigated. The details on these issues are left for future study.

So far, we have written everything in the local coordinate system **n**–**t**–**p** associated with a crack but have not determined this coordinate system yet. The damage criterion defined in (10) should be modified for this purpose. Since that criterion is a result of the transformation of the dissipation potential (see Nguyen (2005) for details), it is in fact the dissipation d_{d} in (2) that should be amended. Omitting unnecessary intermediate details, we can make a direct transition to the damage criterion in its general form (13). The orientation of a crack here is determined based on that damage criterion, in which function F_2 plays an important role. Unlike in (13), where $F_2(\boldsymbol{\sigma})$ is simply a scalar-valued function independent of any directions, $F_2 = F_{2n}(\mathbf{n}, \boldsymbol{\sigma})$ is now defined as a stress- and direction-based function. The modified damage criterion becomes

$$y_{\mathrm{d}} = \max_{\forall \mathbf{n}} F_{2n}(\mathbf{n}, \boldsymbol{\sigma}) - F_1(\alpha_{\mathrm{d}}) = 0 \tag{19}$$

As can be seen, the stress-based damage criterion now gives us the orientation of a crack that maximizes function $F_2 = F_{2n}(\mathbf{n}, \boldsymbol{\sigma})$. This crack orientation generally depends on the stress state of a material point and should reflect the experimental observations (Fig. 2). Earlier work by Schreyer (2007) could be adapted here for a possible form of function $F_{2n}(\mathbf{n}, \boldsymbol{\sigma})$. Nevertheless, the specific forms of functions $F_1(\alpha_{\mathrm{d}})$ and $F_{2n}(\mathbf{n}, \boldsymbol{\sigma})$ for anisotropic cases remain to be determined.

2.3. Non-local regularization

To deal with softening-related problems, the local constitutive model described in Section 2.1 needs to be regularized using non-local theories. Following Pijaudier-Cabot and Bazant (1987), it is necessary to apply non-local treatment only to variables or quantities directly controlling the softening process. With damage-induced softening in the constitutive model, the damage criterion (13) should be formulated as a non-local criterion. In particular, the non-local regularization operator L is applied to the energy term $F_2(\sigma_{ij})$ in the damage criterion as follows:

$$\widetilde{F}_2(\mathbf{x}) = L(F_2(\sigma_{ij})) = \frac{1}{G(\mathbf{x})} \int_{V_{\mathrm{d}}} g(\|\mathbf{y} - \mathbf{x}\|) F_2(\sigma_{ij}(\mathbf{y})) \mathrm{d}V_y \tag{20}$$

where V_{d} is as a volume defined by a sphere of centre $\mathbf{x}$ and radius R; $G(\mathbf{x}) = \int_{V_{\mathrm{d}}} g(\|\mathbf{y} - \mathbf{x}\|) \mathrm{d}V_y$ is used to normalize the weighting scheme applied to the energy-like term in (20); and $g(\|\mathbf{y} - \mathbf{x}\|)$ is the bell-shaped weight function defined by

$$g(r) = g(\|\mathbf{y} - \mathbf{x}\|) = \begin{cases} 0 & \text{if } r > R \\ \left(1 - \dfrac{r^2}{R^2}\right)^2 & \text{if } r \leqslant R \end{cases} \tag{21}$$

From 13, 14 and 20, we obtain the non-local form of the damage criterion:

$$y_{\mathrm{d}} = \frac{1}{G(\mathbf{x})} \int_{V_{\mathrm{d}}} g(\|\mathbf{y} - \mathbf{x}\|) \frac{(1 + p_{\mathrm{t}}) \sigma_{ij}^{+} \sigma_{ij}^{+} - p_{\mathrm{t}} \langle \sigma_{kk} \rangle \langle \sigma_{ll} \rangle}{2E(1 - \alpha_{\mathrm{d}})^2} \mathrm{d}V_y - F_1(\alpha_{\mathrm{d}}) = 0 \tag{22}$$

As can be seen, the above weight function only depends on the distance between points within the volume V_{d}. The non-local interaction radius R therefore acts as a length parameter helping to prevent the localization of deformation into an

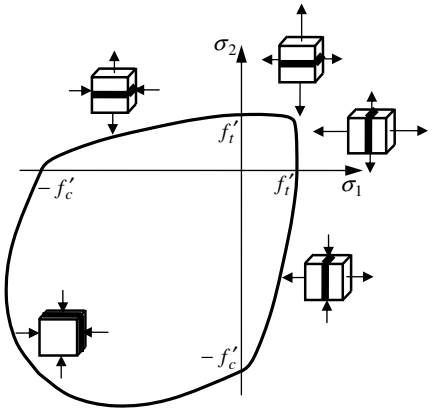

Fig. 2. Damage surface and crack orientations in biaxial loading (adapted from Schreyer (2007)).

infinitesimally small zone. However, a more rational definition of the length parameter accounting for different types of weight function $g(r)$ in non-local models can be expressed as (Jirásek, 1998):

$$l = \sqrt{\frac{\int_0^\infty r^2 g(r)\mathrm{d}r}{\int_0^\infty g(r)\mathrm{d}r}} \tag{23}$$

For the bell-shaped weight function used in this study, Eq. (23) gives $l = R/\sqrt{7}$.

The constitutive behaviour of the non-local model is governed by the following relations: the stress–elastic strain relationship, yield and non-local damage loading functions all of which can be rewritten as

$$\varepsilon_{ij} = \frac{D_{ijkl}\sigma_{kl}}{1-\alpha_\mathrm{d}} + \alpha_{ij} \tag{24}$$

$$y_\mathrm{p}^* = \beta\sigma_{kk} + \sqrt{\frac{\sigma'_{ij}\sigma'_{ij}}{2}} - k = 0 \tag{25}$$

$$y_\mathrm{d} = \frac{1}{G(\mathbf{x})}\int_{V_\mathrm{d}} g(\|\mathbf{y}-\mathbf{x}\|)\frac{(1+p_\mathrm{t})\sigma_{ij}^+\sigma_{ij}^+ - p_\mathrm{t}\langle\sigma_{kk}\rangle\langle\sigma_{ll}\rangle}{2E(1-\alpha_\mathrm{d})^2}\mathrm{d}V_y - F_1(\alpha_\mathrm{d}) = 0 \tag{26}$$

The numerical implementation of this kind of model has been presented in Nguyen (2005).

3. Determination of model parameters

The calibration of parameters for non-local models has been discussed by several researchers (Bazant and Pijaudier-Cabot, 1989; Jirásek, 1998; Carmeliet, 1999; Mahnken and Kuhl, 2003; Ferrara and Di Prisco, 2001; Le Bellego et al., 2003; Nguyen, 2005). Their studies can be generally grouped into two classes: those based directly on the numerical inverse analysis of experimental results and those exploiting the correspondence between the cohesive crack model and crack band model. A comprehensive review and classification of regularization methods (e.g. cohesive crack model, crack band approach and non-local regularization techniques) can be found in Jirásek and Patzák (2001). In the first kind of parameter identification, automatic calibration of model parameters based on numerical inverse analysis is employed. This kind of automatic calibration procedure uses optimization algorithms, experimental data from real structural tests and size effect laws. Several different optimization algorithms have been used in Carmeliet (1999), Mahnken and Kuhl (2003) and Le Bellego et al. (2003). For computational efficiency, the initial set of model parameters, as an initial guess, can be determined based on the size effect law and experimental tests of several geometrically similar specimens with different dimensions (Carmeliet, 1999; Le Bellego et al., 2003). In this method, the length parameter l and the parameters of the local constitutive model are treated equally as general parameters of the non-local constitutive equations in a boundary value problem. Therefore, the correlation between local constitutive behaviour and the length parameter is not specifically addressed and exploited. This, along with the complications and expense of solving the inverse problem, makes the method difficult to apply in practice.

The second kind of parameter identification procedure is pursued in this study. The correspondence between the cohesive crack model and crack band model (see Mazars and Pijaudier-Cabot, 1996; Bazant, 2002; Elices et al., 2002 for details) along with a relationship between the length parameter l of non-local model and the width w_t of an imaginary and uniformly damaged crack band is exploited. The crack band width w_t, also termed the dissipation length (Jirásek, 1998) is different from the actual width z_t of the micro-cracked zone in continuum models. This width w_t defines the minimum size of a volume element, above which the material can be considered as homogeneous (Bazant and Oh, 1983). Fig. 3 illustrates the difference between w_t and the actual width z_t of the micro-cracked zone in non-local models. It can readily be seen in the figure that these two widths coincide in crack band models with a constant damage/strain distribution across the crack band width.

In the calibration of model parameters, the correspondence between cohesive crack model and crack band model has been widely adopted (e.g. in non-local and gradient models used by De Borst and Pamin, 1996; Di Prisco et al., 2000; Ferrara and Di Prisco, 2001; Meftah and Reynouard, 1998; Jirásek, 1998; Jirásek et al., 2004). Moreover, it is also backed by experimental data for fracture energy, as well as by testing methods to measure the fracture properties of the material (e.g. the work of fracture method, size effect method). For that reason, it is adopted in this study for the calibration of model parameters for non-local coupled damage-plasticity models.

Following this correspondence, the displacement jump (or fictitious crack opening) u in the cohesive crack model is smeared out over the crack bandwidth w_t in a continuum model (see Fig. 4 for details). This transforms the experimentally derived stress–separation law in the cohesive crack model into the stress–strain relationship in a continuum model and helps to determine parameters governing the local constitutive behaviour. This transformation is to give the local constitutive relation a response consistent with the length parameter l, cohesive crack properties (including the fracture energy G_F and the stress–separation curve), and crack bandwidth w_t. The local constitutive behaviour of the model in this case is directly affected by the choice of the length parameter of the model. As the cohesive crack model is used as a basis for parameter identification in the non-local model, its corresponding properties should be properly identified and determined. A fully experimental method (e.g. the work of fracture method by Petersson, 1981; Bazant, 1996) or an indirect method (Tin-loi and Que, 2001; Que and Tin-loi, 2002) using both numerical procedures and experimental data can be used for this purpose. In

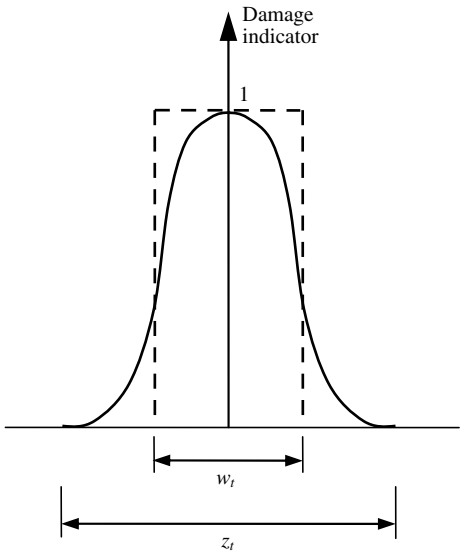

Fig. 3. Damage profile in uniaxial test using non-local model, and definition of w_t and z_t (adapted from Bazant and Pijaudier-Cabot, 1989).

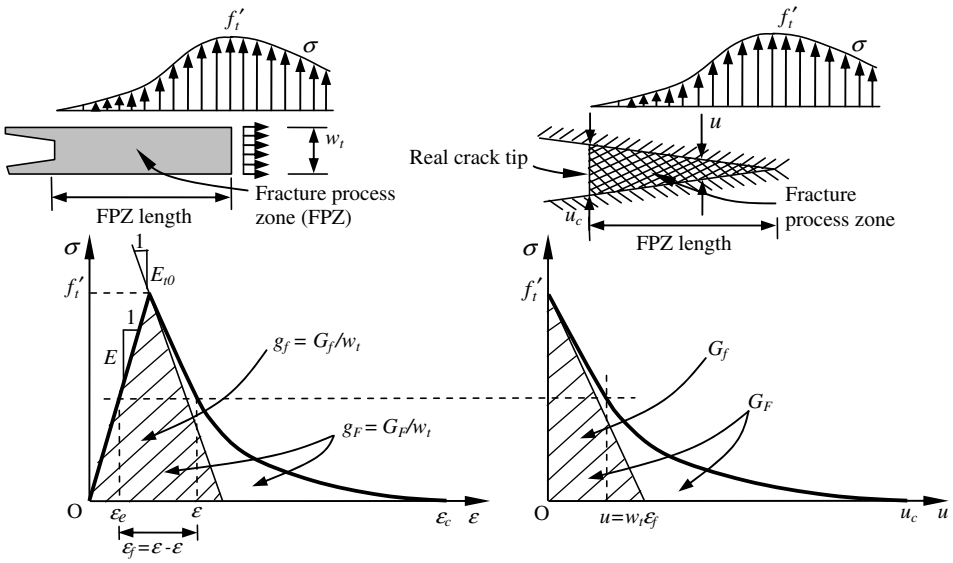

Fig. 4. The correspondence between (a) the stress–strain relation in crack band model, and (b) the stress–separation law in cohesive crack model; after Bazant (2002) and Elices et al. (2002).

this paper, for the sake of simplicity, it is assumed that a cohesive stress–separation law and its properties are known for the material to be modelled.

As discussed, the crack bandwidth w_t is needed for the transformation from the cohesive stress–separation law to the stress–strain law in continuum models. Unlike in crack band approach, where a linear relationship between w_t and the finite element size h can be used to identify a local constitutive law (Bazant and Oh, 1983), the length parameter l in a non-local model is not linearly proportional to w_t. Their relationship is non-linear, dependent on several parameters of the non-local model, and therefore should be appropriately determined to give the local constitutive law a response consistent with the choice of the length parameter l. In the next section, the identification and determination of parameters for local constitutive law is presented, based on the assumption that the imaginary width w_t of the fracture process zone is known in advance. This is then followed by a procedure for the determination of the relationship between w_t and the non-local interaction radius R. It will be shown that mutual influence effects between local and spatial sets of parameters are fully accounted for through the proposed procedure.

3.1. Parameters governing the local constitutive behaviour

The calibration of model parameters here is based on uniaxial tensile test, and has been briefly presented in Nguyen and Korsunsky (2006) and also Nguyen and Houlsby (2008a). It is therefore described here only for the sake of completeness. The uniaxial stress–strain curve needed for the determination of model parameters is obtained from the stress–separation law in the cohesive crack model and the width w_t of the fracture process zone (Fig. 4).

In the one-dimensional formulation the energy function (1) and the dissipation function (2) assume the following simplified forms:

$$g = \frac{-\sigma^2}{2E(1-\alpha_d)} - \sigma\alpha_p \text{ and} \tag{27}$$

$$d = F_1(\alpha_d)\dot{\alpha}_d + (1-\alpha_d)(f'_t + H_t\alpha_p)\dot{\alpha}_p \tag{28}$$

where both the plastic strain tensor α_{ij} and the equivalent plastic strain ε_p are assumed to reduce to α_p such that $\alpha_p \geqslant 0$ and $\dot{\alpha}_p \geqslant 0$ in uniaxial tension. The local constitutive relations (8–10) now become

$$\varepsilon = \frac{\sigma}{E(1-\alpha_d)} + \alpha_p \tag{29}$$

$$y_p = \sigma - (1-\alpha_d)(f'_t + H_t\alpha_p) = 0 \tag{30}$$

$$y_d = \frac{\sigma^2}{2E(1-\alpha_d)^2} - F_1(\alpha_d) = 0 \tag{31}$$

where the function $F_1(\alpha_d)$ and its two parameters E_{pt} and n_t have been defined in (15). The effect of model parameters on the stress–strain response can be found in Nguyen (2005) and Nguyen and Houlsby (2008a).

In principle it is possible to obtain the stress σ, the tensile damage indicator α_d and the plastic strain α_p analytically from the system (29–31), in terms of the total strain ε. Unfortunately, in practice this is not always possible since the solution of the system (29–31) depends strongly on the choice of function $F_1(\alpha_d)$. It turns out to be easier to perform the necessary mathematical manipulations with respect to the damage indicator α_d as the principal variable. Omitting the details of mathematical manipulations we write

$$\sigma = (1-\alpha_d)\sqrt{2EF_1(\alpha_d)} \tag{32}$$

$$\alpha_p = \frac{1}{H_t}\sqrt{2EF_1(\alpha_d)} - \frac{f'_t}{H_t} \tag{33}$$

$$\varepsilon = \frac{E+H_t}{H_t}\sqrt{\frac{2F_1(\alpha_d)}{E}} - \frac{f'_t}{H_t} \tag{34}$$

The total dissipated energy due to the combination of damage and plasticity can be obtained by direct integration of the dissipation rate in Eq. (28), after substituting (33) and its derivative with respect to α_d into (28). Denoting by D_d and D_p the total energy amounts dissipated due to damage and plastic-frictional processes, respectively, we have

$$D_d = \int_0^1 F_1(\alpha_d)\mathrm{d}\alpha_d = \frac{f'^2_t}{2E} + \int_0^1 (1-\alpha_d)\frac{\partial F_1}{\partial \alpha_d}\mathrm{d}\alpha_d \tag{35}$$

$$D_p = \int_0^\infty (1-\alpha_d)(f'_t + H_t\alpha_p)\mathrm{d}\alpha_p = \frac{E}{H_t}\int_0^1 (1-\alpha_d)\frac{\partial F_1}{\partial \alpha_d}\mathrm{d}\alpha_d \tag{36}$$

The total dissipated energy D is the sum of the energies dissipated due to damage and plasticity. This total dissipated energy is in fact the volumetric fracture energy g_F and can also be obtained as the area under the stress–strain curve (Fig. 4; see also Nguyen (2005)). Thus

$$g_F = D = D_d + D_p = \frac{f'^2_t}{2E} + \frac{E+H_t}{H_t}\int_0^1 (1-\alpha_d)\frac{\partial F_1}{\partial \alpha_d}\mathrm{d}\alpha_d \tag{37}$$

The interpretation of experimental results leads to the conclusion that g_F consists of two parts, g_{pF} that is due purely to fracture processes, and $(g_F - g_{pF})$ that is due to plastic frictional mechanisms (Bazant, 1996). This observation is used here for the determination of model parameters. According to Bazant (1996, 2002), the value of g_{pF} is about 0.2–0.5 of g_F, which means that the major part of energy dissipation comes from plastic-frictional mechanisms.

The shape of the stress–separation curve can be used to provide additional input for the calibration process. The experimentally determined fracture energy G_F can be considered to consist of two parts, corresponding to the peak (G_f) and tail $(G_F - G_f)$ responses of the material (Bazant, 2002). By way of interpretation, the area determined from the tangent of the non-linear stress–strain curve at peak stress (the hatched area in Fig. 4a) is written as $g_f = G_f/w_t$ and taken to be equal to tg_F. The value of the fraction t lies in the range of 0.1–0.3 and depends on the tensile strength f'_t, fracture energy G_F of the material, and the crack bandwidth w_t (Nguyen, 2005).

The initial tangent modulus E_{t0} at peak stress (Fig. 4a) is needed to determine the initial volumetric fracture energy g_f. This modulus can be obtained by differentiating (32) and (34) and substituting $\alpha_d = 0$ into the obtained expression:

$$E_{t0} = -\frac{E_{pt}H_t}{E + H_t} \tag{38}$$

Therefore we have the following system of equations for the determination of model parameters:

$$g_F = D = D_d + D_p = \frac{f_t'^2}{2E} + \frac{E + H_t}{H_t}\int_0^1 (1 - \alpha_d)\frac{\partial F_1}{\partial \alpha_d}\mathrm{d}\alpha_d \tag{39}$$

$$g_{pF} = D_d = \int_0^1 F_1(\alpha_d)\mathrm{d}\alpha_d = \frac{f_t'^2}{2E} + \int_0^1 (1 - \alpha_d)\frac{\partial F_1}{\partial \alpha_d}\mathrm{d}\alpha_d \tag{40}$$

$$g_f = tg_F = \frac{f_t'^2}{2}\left(\frac{1}{E} + \frac{E + H_t}{E_{pt}H_t}\right) \tag{41}$$

The above system of non-linear equations can be solved numerically, e.g. using a Matlab code. A simple numerical example is given here to demonstrate the proposed procedure for the parameter identification. The following material properties were used: Young's modulus $E = 38,000\ \mathrm{N/mm^2}$, tensile strength $f_t' = 3\ \mathrm{N/mm^2}$, fracture energy $G_F = 0.125\ \mathrm{N/mm}$, and crack bandwidth $w_t = 20\ \mathrm{mm}$.

The effects of the ratio g_{pF}/g_F on model parameters and stress–strain behaviour are illustrated in Figs. 5 and 6. Plasticity-dominated response can be obtained by using $g_{pF}/g_F = 0$ ($H_t = 0$ in this case), while damage-dominated response is recovered by setting $g_{pF}/g_F = 1$ ($H_t = \infty$ in this case). In all cases (Fig. 6b) the total fracture energy g_F remained unchanged (see Eqs. (39) and (40)). We note that the experimentally observed value of the ratio g_{pF}/g_F is between 0.2 and 0.5 (Bazant, 1996 and Bazant, 2002), resulting in coupled damage-plasticity behaviour (Fig. 6b). It should also be noted here that a perfect case with plasticity being the only dissipation mechanism cannot be derived from the coupled model presented above, as the softening behaviour of the model is mainly governed by damage mechanism. However, a nearly perfect case with $H_t \approx 0$ can be used to derive models with plasticity-dominated responses (Fig. 6b). Furthermore, the advanced feature of the presented calibration procedure, compared to other simple methods (e.g. in Jefferson, 2003a; Grassl and Jirasek, 2006), is that the link between model parameters and the physical dissipation processes can be explicitly established and confirmed by experiments.

3.2. Parameter governing the spatial interaction

The calibration of the length parameter governing the spatial interaction of material points was developed in Nguyen (2005). It has been applied with success to pure damage models (Nguyen and Houlsby, 2007) and coupled damage-plasticity models (Nguyen, 2005). In this section, for completeness only brief details of the method will be described. Further details featuring a more complete literature review can be found in Nguyen (2005) and Nguyen and Houlsby (2007).

From Section 3.1, it can be seen that the parameters governing the local constitutive behaviour of a non-local model are dependent on the imaginary width w_t of the fracture process zone. In the crack band approach, as strain localizes in one element, the finite element size h needs to be proportional to w_t by a readily determined proportional constant (e.g. $w_t = \sqrt{2A}$ for a linear element, with A being the area of the element; in Rots (1988), Feenstra and de Borst (1995)). Otherwise, the stress–strain softening curve of the local constitutive model must be adjusted to assure the right amount of dissipation specified by the fracture energy G_F (Bazant and Oh, 1983; Bazant and Cedolin, 1991 (Chapter 13)).

Nevertheless, in non-local analysis the width of the localization zone, defined by z_t (see Fig. 3), may contain several softened finite elements with different constitutive behaviour due to the non-local averaging process. As an illustration, Fig. 7 shows the results obtained from the non-local numerical analysis of a bar under tension. A defect in the bar is created next to

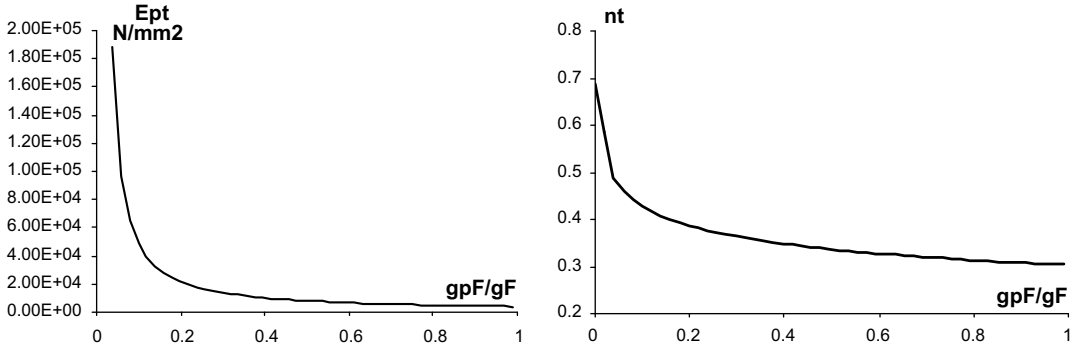

Fig. 5. The dependence of damage parameters E_{pt} and n_t on the ratio g_{pF}/g_F.

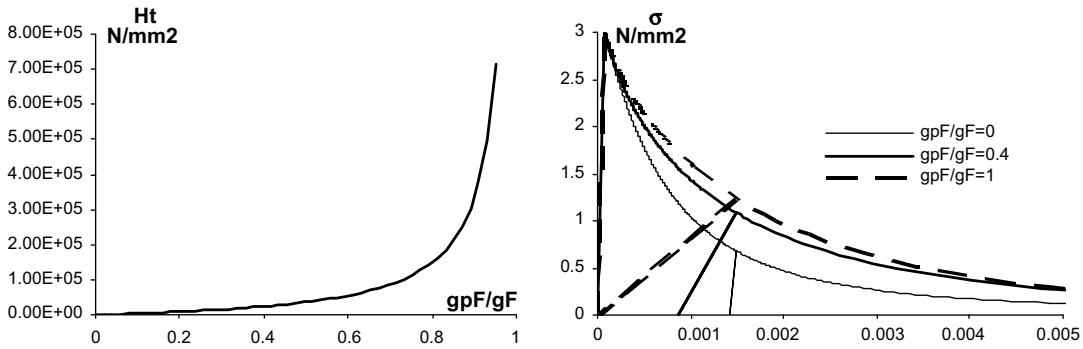

Fig. 6. The effect of the ratio g_{pF}/g_F (a) on the hardening modulus H_t, and (b) on the stress–strain behaviour of the model.

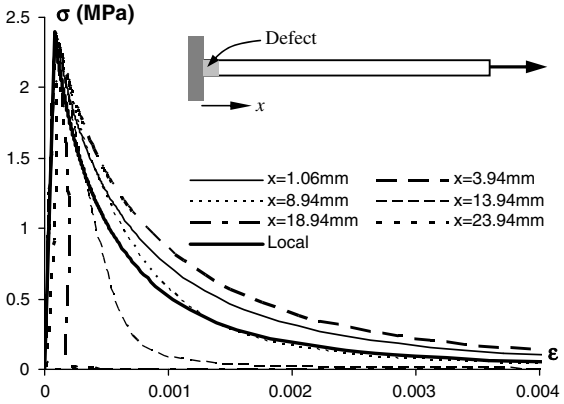

Fig. 7. Stress–strain curves at points in the damaged zone of a bar in a non-local analysis.

the clamp to trigger damage and softening. As can be seen in Fig. 7, the obtained stress–strain curves are different at points inside the damaged zone and different from the local behaviour of the material model used in the numerical analysis. The amounts of dissipated energy (as area under the stress–strain curve) vary along the bar length. The imaginary crack band width w_t in this case significantly depends on the length parameter l ($l = R/\sqrt{7}$ in our non-local model) and other parameters of the local constitutive model (Jirásek, 1998). In other words, w_t in non-local models is governed by both the length l and the local constitutive behaviour of the model. It is therefore difficult, even impossible, to determine the relationship between w_t and the length parameter l analytically in non-local models, except in some simple cases with a linear softening law (e.g. in De Borst and Muhlhaus, 1992; Meftah and Reynouard, 1998; Zhao et al., 2005).

For that reason, a condition on the equivalence between the energy dissipated by a non-local model with imaginary crack bandwidth w_t and that specified by the fracture energy G_F is used in this study. Non-local numerical analyses of a simple bar under uniaxial tension will be carried out for the determination of a relationship between w_t and the internal length l of the non-local model. Once this relationship is established, choice of l to yield a numerical crack band width w_t close to that proposed in the literature (e.g. $w_t \approx 3d_{max}$ in Bazant and Oh, 1983 and Bazant and Pijaudier-Cabot, 1989) is readily determined.

In the numerical analysis, we assume here that w_t is proportional to the interaction radius R by the ratio $k = w_t/R$. This is practically reasonable, as the dependence of w_t on other parameters of the model is implicitly embedded in the procedure proposed here. The relationship between g_F and G_F can be rewritten as

$$G_F = w_t g_F = kRg_F \tag{42}$$

where k is the unknown ratio to be determined. The initial value of k can be chosen, depending on the type of non-locality (e.g. non-local strain, or non-local damage energy; k has been numerically found to be in the range of 1–3 for the non-local model in this study). For an assumed value of k, denoted here as k'', and a fixed value of radius R, the assumed crack band width w_t'' is obtained as $w_t'' = k''R$. The volumetric fracture energies g_F and g_f can then be determined from Eq. (42), using $w_t'' = k''R$, followed by the determination of all parameters of the model based on Eqs. (39)–(41). With all parameters in hand, we can then carry out a numerical failure analysis of a one-dimensional bar with a defect at its middle to trigger damage, and obtain the total dissipation as the area under the load–displacement curve. In principle, the numerically obtained dissipated energy per unit area G_F', should coincide with G_F, representing the right amount of energy dissipated per unit area during the fracture process. On the other hand, the numerically calculated width w_t' of the fracture process zone, determined by the

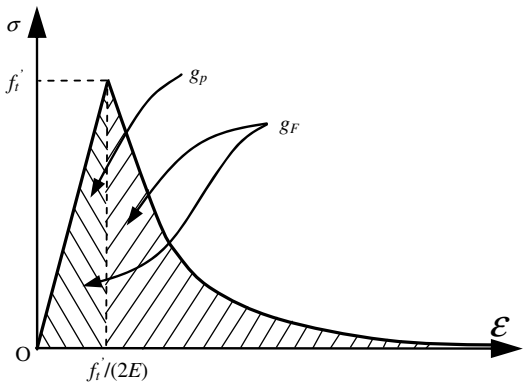

Fig. 8. Definition of the ductility parameter η.

ratio G_F'/g_F with g_F obtained from Eq. (42), should match its assumed value $w_t'' = G_F/g_F$. Alternatively, $k'' = w_t''/R$ and $k' = w_t'/R$ should coincide. However, this is not always the case and the procedure should be repeated several times until the balance of dissipated energy is established.

In the method proposed here, no iteration is needed. In addition, relationships between non-dimensional quantities are used to make the process of determining the ratio k easier. Jirásek (1998) suggested using the relationships between the ductility parameter η ($\eta = g_F/g_p$; $g_p = f_t'^2/2E$; see Fig. 8) and the relative dissipation length w_t/l for the calibration. However, for the use of the bell-shaped function in this study, $k = w_t/R$ is adopted as the relative dissipation length.

For a fixed value of non-local interaction radius R, there are two separate values of the relative dissipation lengths: $k'' = w_t''/R$ and $k' = w_t'/R$, obtained from the assumed width w_t'' and the numerically calculated width w_t' of the fracture process zone, respectively. For the right amount of dissipation, these two values of k'' and k' must coincide (see Fig. 9). Two curves ($k''(\eta)$ and $k'(\eta)$) in Fig. 9 represent the variation of k'' and k' with respect to changes in the ductility parameter η. From Eq. (42) and the definition $\eta = g_F/g_p$, we obtain $k''(\eta) = 2EG_F/(\eta R f_t'^2)$, while the shape of $k'(\eta)$ is generally obtained from the numerical failure analysis of a one-dimensional bar with a defect at its middle (see Jirásek, 1998). The proposed procedures can be summarized as follow:

- Assume values of k_i'''s: $k_1'' = 1.0, \ldots, k_n'' = 3.0$ for the damage model in this study.
- Calculate the fracture energies $g_{Fi} = G_F/(k_i'' R)$, ductility parameters $\eta_i = g_{Fi}/g_p$ (see Fig. 8) and determine the corresponding sets of parameters for local damage model, based on Eqs. (39)–(41).
- Carry out the numerical analyses of a one-dimensional bar and calculate the corresponding total dissipated energies D_i as the areas under the load–displacement curves.
- From the obtained dissipated energies, calculate the corresponding fracture energies $G_{Fi}' = D_i/A$, where A is the cross-sectional area of the bar, and derive the ratios $k_i' = G_{Fi}'/R g_{Fi}$.
- The correct value of k will be found by plotting k_i'' and k_i' against $\eta_i = g_{Fi}/g_p$ and determining the intersection point of the two plotted curves (see Fig. 9).

A literature review on the determination of the ratio $k = w_t/R$ along with further details on the procedure and corresponding numerical illustrations for pure damage models can be found in Nguyen (2005) and Nguyen and Houlsby (2007).

4. Numerical examples

This section is dedicated to the numerical validation of the proposed non-local coupled damage-plasticity model and the corresponding calibration procedure for model parameters. All the numerical analyses were carried out using the local arc-length control (May and Duan, 1997) for the incremental analysis, and Newton–Raphson method for the iterative technique. Finite element meshes of six-node triangular elements were used in all examples. The convergence tolerance parameter was 10^{-4} for the norm of the out-of-balance force vector in the Newton–Raphson iterative process. The same tolerance was used in the stress update routine to gauge the errors occurring in returning the stresses to the loading surfaces. Automatically chosen numbers of increments (see May and Duan, 1997; Crisfield, 1997, Chapter 9, volume 1), controlled by the number of iterations required for each load increment, were applied throughout the examples. Due to the complexity of the non-local model and implicit damage evolution law in this study, a non-local consistent stiffness matrix (e.g. that in Jirásek and Patzák (2002)) was unfortunately not available. Instead, a local stiffness matrix secant with respect to damage and tangent with respect to plasticity (see Nguyen (2005) for details) was used in all numerical examples. A loading scheme consisting of three load stages (first: fully elastic behaviour, second and third: peak and post-peak stages) was employed, in which the controlling minimum and maximum numbers of iterations for the last two stages were normally 12–18 and 18–27, respectively.

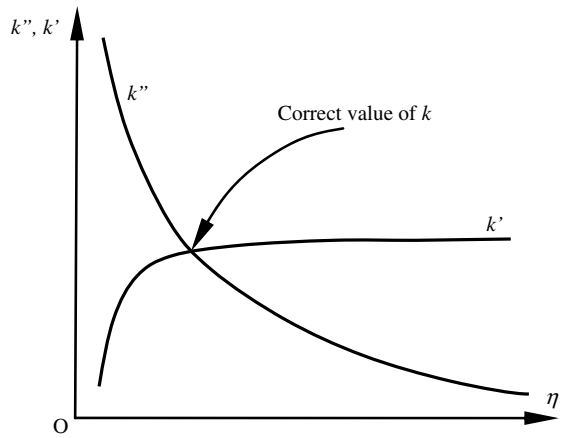

Fig. 9. Determination of the ratio $k = w_t'/R$.

The rate of convergence was rather low, mostly due to the time spent on the solution of non-local coupling equations (between integration points) during the stress update process. This is likely unavoidable for the model used here.

4.1. Three-point bending test of Petersson

The numerical simulation of a notched beam in a three point bending test (Petersson, 1981) is presented in this section to demonstrate the calibration procedure in Section 3. The material properties were taken from the experimental test of Petersson (1981): $E = 30,000$ MPa, $\nu = 0.2$, $f_t' = 3.33$ MPa, $G_F = 0.124$ N/mm, $d_{max} = 8$ mm. Only pure damage behaviour was considered. A simple test (Fig. 10) was set up for the determination of model parameters. A 1% reduction of the damage ultimate tensile stress f_t' was introduced to the shaded element in the figure, aiming to trigger softening in that element.

The calibration results are shown in Fig. 11, with the obtained values of k corresponding to the assumed values of the non-local interaction radius R. It can be seen that k tends to increase for decreasing value of R. The above calculation of k and determination of model parameters can be readily verified by carrying out the numerical analysis of the corresponding three point bending test. The finite element meshes contain six-node triangular elements (Fig. 12). The corresponding model parameters (E_{pt} and n_t) are obtained from (39) and (41), with $H_t = \infty$ for damage-dominated behaviour, and shown in Table 1.

From the obtained numerical results (Fig. 13), it is seen that the numerical load–deflection curves match rather well the experimental ones, verifying the total dissipated energy in mode I fracture. The obtained load–deflection curves are objective

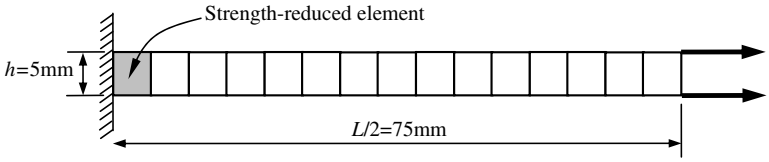

Fig. 10. Finite element model used for the determination of parameter k.

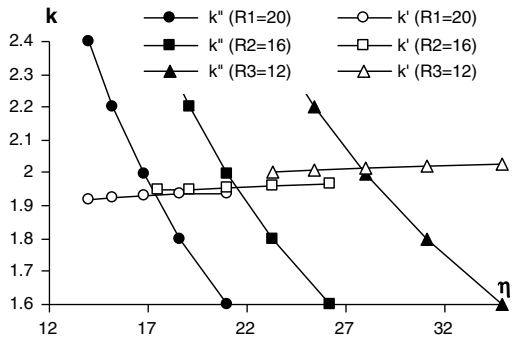

Fig. 11. Determination of parameter k.

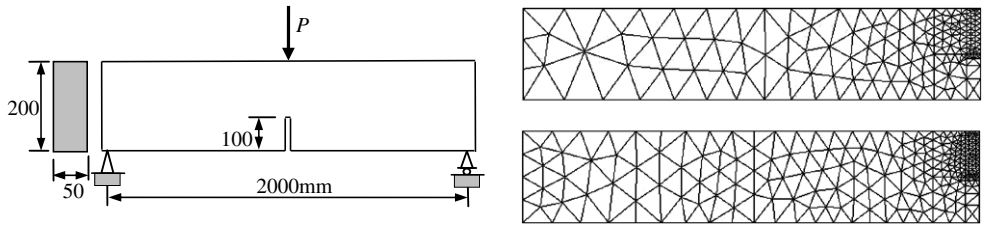

Fig. 12. Three-point bending test: geometrical data, and FE meshes of half beam model.

Table 1
Parameters of local model corresponding to choice of non-local radii – bending tests

Non-local radius	Model parameters		
	k	E_{pt} (MPa)	n_t
$R_1 = 2.5d_{max}$	1.93	8967.34	0.34
$R_2 = 2.0d_{max}$	1.96	6898.61	0.32
$R_3 = 1.5d_{max}$	2.02	5067.76	0.30

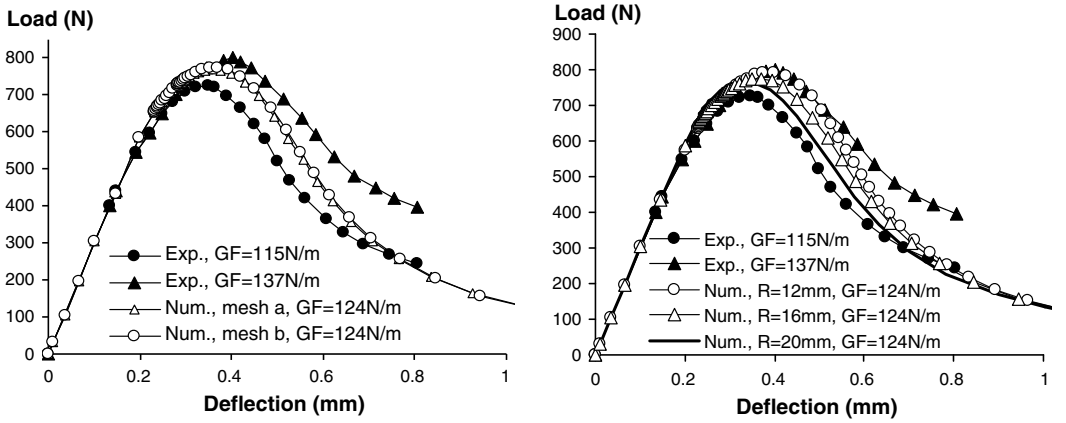

(a) Use of different FE meshes (b) Use of different parameter sets

Fig. 13. Load–deflection curves, three point bending test of Petersson (1981).

with respect to the choice of the numerical discretization (Fig. 13a). It can also be seen that the load–displacement curves obtained from the numerical analyses using different non-local interaction radii are very close (Fig. 13b).

The slight differences in the numerical peak loads (Fig. 13b) come from the use of numerical analyses of a simple bar to determine the ratio k. The constant distribution of uniaxial stress in the bar used (Fig. 10) is obviously different from that in the three-point bending test, where high gradients of stresses occur at the notch tip and affect the onset of damage when using different non-local radii. This is due to the non-local averaging of stress-dependent energy-like term in the non-local damage loading function (26). Better numerical responses, in which the differences of the results from the use of different non-local radii are reduced, can in principle be achieved if one adopts the three-point bending test to calibrate the model parameters. In other words, the same procedures for the determination of parameters can be carried out based on the three-point bending test, instead of the uniaxial test used here. It would therefore be required that the numerical failure analysis of the three-point bending test be carried out until very late stages (e.g. very low load carrying capacity of the beam), which is of course a difficult computational problem and hence not practical. Therefore, the use of complicated tests is not recommended in this study. In addition, better numerical responses can in principle be achieved through optimization procedures combined with size effect tests on specimens of different sizes. This is, however, outside the scope of this study.

4.2. Tension test

In this numerical example, the numerical simulations of a double edge notched specimen under tension (Shi et al., 2000) are presented (Fig. 14a). In the numerical models, the specimen is fixed in both directions at the bottom edge, and in horizontal direction at the top edge. The numerical analyses were carried out using four meshes of 6-node triangular finite elements (Fig. 14b), with prescribed vertical displacements at the top edge of the specimen.

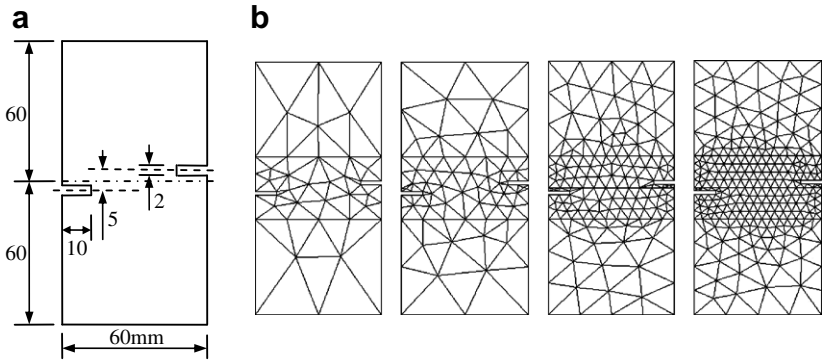

Fig. 14. Double edge notched specimen (10 mm thick): geometry (a) and FE meshes (b).

For no data on the unloading path, it is assumed here that only tensile damage mechanism is activated, resulting in a pure non-local damage model. The material properties used are: Young's modulus $E = 24$ GPa, Poisson's ratio $v = 0.2$, tensile strength $f_t' = 2.4$ MPa, fracture energy $G_f = 0.059$ N/mm, and maximum aggregate size $d_{max} = 8$ mm. In the numerical simulations, two different values of non-local interaction radius were used: $R_1 = 2.0d_{max} = 16$ mm and $R_2 = 1.0d_{max} = 8$ mm.

The procedure described in Section 3 was used to determine the values of the ratio k corresponding to two different non-local radii. Fig. 15 and Table 2 show the graph used in the determination of parameters, and the obtained values of those model parameters, respectively. Two different values of k were obtained, again showing the need for the proper determination of model parameters for every given value of non-local radius R.

The regularization effect of the non-local model is illustrated in Fig. 16(a), with results from runs using different FE meshes almost coincident. On the other hand, the load–displacement curves obtained from two numerical analyses using two different values of non-local interaction radius R show good agreement in shape with the experimental counterpart (see Fig. 16b). Only the peak loads slightly differ from one another and from the experimental one.

4.3. Four-point bending test of a notched beam under cyclic loading

In this example, the four-point bending test experimentally performed by Hordijk (1991) is simulated using the proposed non-local coupled damage-plasticity model. The geometry of the specimen and finite element meshes of a half-beam model are depicted in Fig. 17. The following material properties were given (Hordijk, 1992): $E = 38,000$ MPa, $v = 0.2$, $f_t' = 3.0$ MPa, $G_F = 125$ N/m, with the assumed ultimate stress in uniaxial compression $f_c' = 30$ N/mm^2.

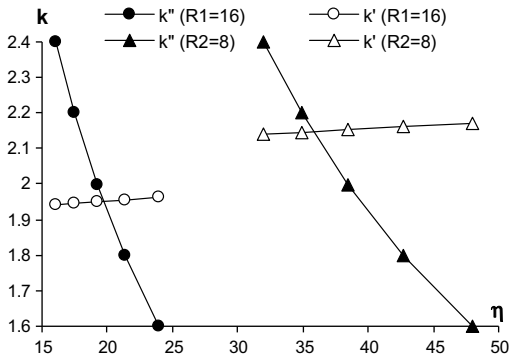

Fig. 15. Determination of parameter k – tension test.

Table 2
Parameters of local model corresponding to choice of non-local radii – tension test

Non-local radius	Model parameters		
	k	E_{pt} (MPa)	n_t
$R_1 = 16$ mm	1.95	7654	0.33
$R_2 = 8$ mm	2.15	3779	0.29

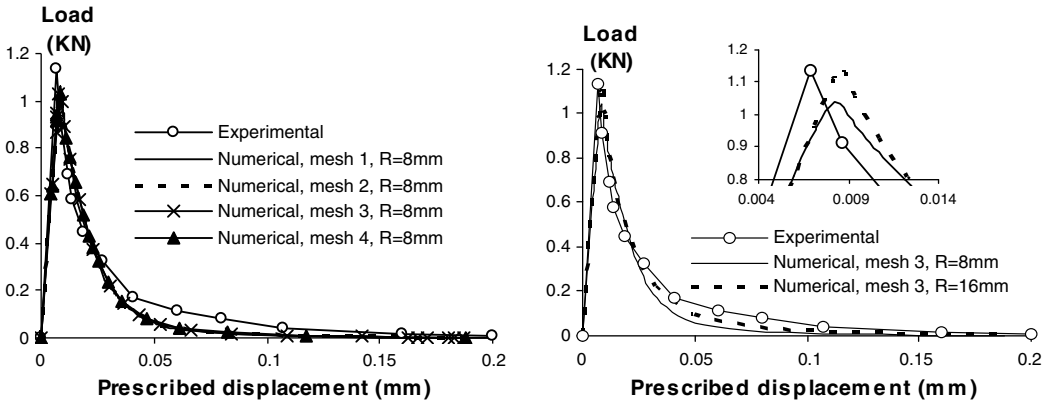

(a) Use of different FE meshes (b) Use of different parameter sets

Fig. 16. Load–displacement curves – tension test.

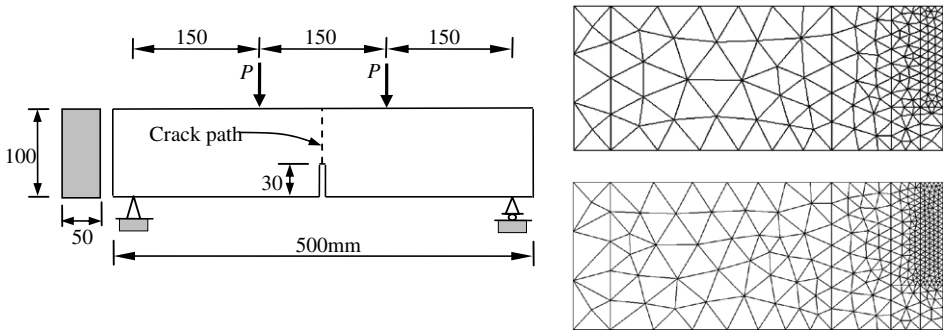

Fig. 17. Four point bending test – geometry and FE meshes.

Again, three different non-local radii and two FE meshes (Fig. 17) were used for the numerical simulations. The ratios $t = G_f/G_F = 0.2$ and $G_{pF}/G_F = 0.48$ were assumed (see Section 3.1). Three parameter sets corresponding to three different non-local radii were obtained using the procedure in Section 3 (see Fig. 18), and shown in Table 3 below.

The load–deflection curves are shown in Fig. 19. It can be seen that all the numerical curves match each other rather well and there is almost no difference in the numerical results using different FE meshes and different non-local radii (Fig. 19). This is an important feature showing both the capability of the proposed calibration procedure and the regularization effect of this non-local model. On the other hand, the difference between results from analyses using pure damage model and coupled damage-plasticity model is marginal (Fig. 19b); only the unloading paths are different. In addition, due to the fixed ratio G_{pF}/G_F used in the calibration, the parameter H_t is almost invariant (relative change of less than 1.5%) with the change of non-local radius (Table 3), and unloading paths from solutions using different radii almost coincide. This result demonstrates the consistency of the proposed calibration procedure.

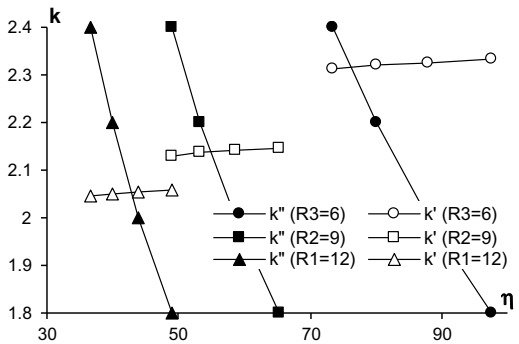

Fig. 18. Determination of parameter k – four-point bending test.

Table 3
Parameters of local model corresponding to choice of non-local radii

Non-local radius	Model parameters			
	k	H_t (MPa)	E_{pt} (MPa)	n_t
$R_1 = 12$ mm	2.05	33,371	10,738	0.35
$R_2 = 9$ mm	2.14	33,745	8098	0.34
$R_3 = 6$ mm	2.32	33,800	6381	0.33

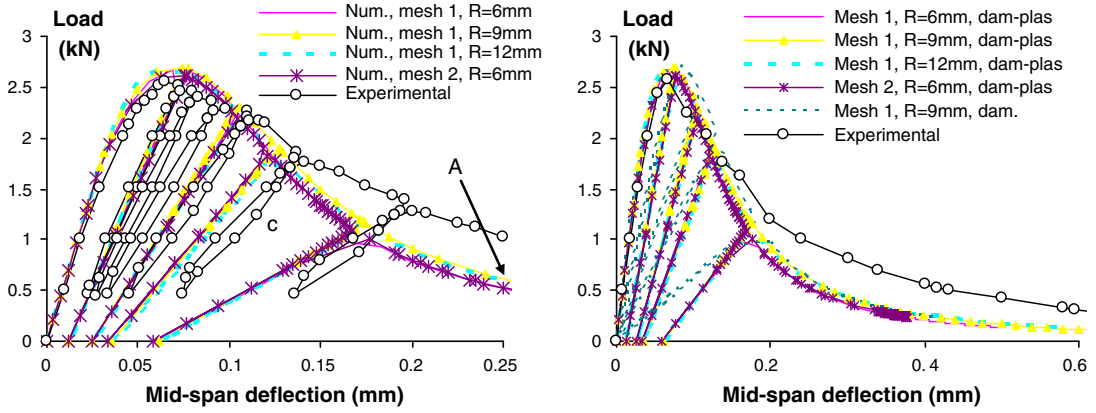

Fig. 19. Four-point bending test – load-deflection curves. Peak (a) and tail behaviour (b).

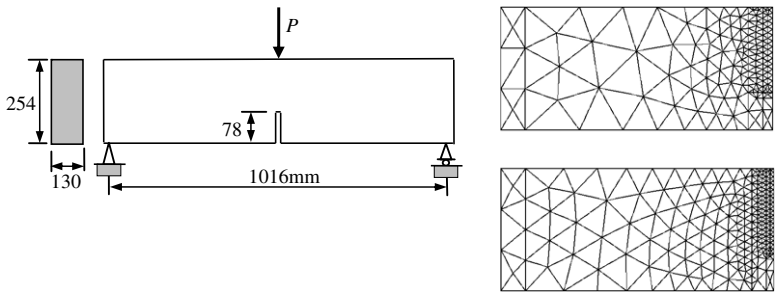

Fig. 20. Geometry and finite element meshes – three-point bending test, cyclic loading.

4.4. Three-point bending test of a notched beam under cyclic loading

This test was experimentally carried out by Perdikaris and Romeo (1995) and has also been used by several researchers (Meschke et al., 1998; Hatzigeorgiou and Beskos, 2002) for the validation of their damage-plasticity constitutive models. The beam geometry and finite element meshes used are depicted in Fig. 20. The following material properties were provided: Young modulus $E = 43,600$ MPa, Poisson's ratio $\nu = 0.2$, tensile strength $f_t' = 4.77$ MPa, compressive strength $f_c' = 63.4$ N/mm^2, fracture energy $G_F = 89.17$ N/m. Three different sets of parameters were used, with same non-local radius $R = 9$ mm (Table 4).

The numerically obtained load–deflection curves are shown in Fig. 21. There is almost no difference between results from the two meshes using the proposed non-local model. In all cases, a good match between numerical and experimental peak-load can be observed. The unloading slopes on the numerical curves (Fig. 21a) are also close to the experimental ones, showing the capability of the numerical models in producing residual deflections at zero-load state. The effect of the ratio g_{pF}/g_F in the model (see Section 3) on the overall responses of the simulated structure is shown in Fig. 21b. It can be seen in the figure that the overall load–deflection curves remains almost unchanged, while the slopes of the unloading curves vary with changes in the ratio g_{pF}/g_F. This trend again clearly demonstrates the consistency of the proposed calibration procedures.

5. Discussion and conclusions

The thermo-mechanical formulation of a coupled damage-plasticity model was presented. This model was used as a means to illustrate some features of the proposed approach, particularly the calibration of model parameters. Both sets of

Table 4
Model parameters corresponding to choice of the ratio g_{pF}/g_F

g_{pF}/g_F	Model parameters			
	k	H_t (MPa)	E_{pt} (MPa)	n_t
0.25	2.06	11,380	58,382	0.42
0.35	2.06	19,838	38,641	0.40
0.45	2.06	31,372	28,877	0.38

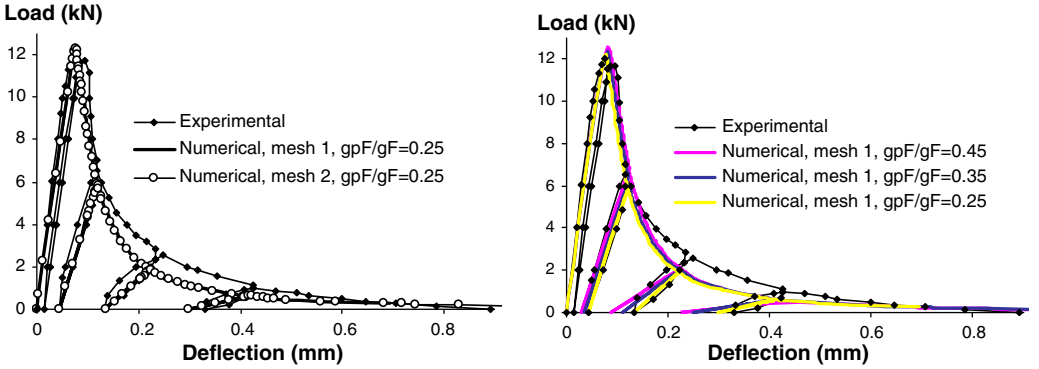

Fig. 21. Load–deflection curves using different FE meshes (a), and different values of g_{pF}/g_F (b).

parameters governing the local constitutive behaviour and non-local interaction of material points were shown to be identifiable, and consistently determined using the procedures presented in this study. The proposed procedures for the calibration of model parameters give the non-local model behaviour consistent with the fracture properties of the material. In other words, the model response due to the change of the length parameter remains almost unchanged (provided all other parameters are adjusted accordingly). As a consequence, several sets of parameters, each corresponding to a particular value of the length parameter, can be obtained based on the proposed method. The choice of the best set of model parameters, with the length parameter being the true characteristic length of the material, can be made based on size effect tests (Carmeliet, 1999; Le Bellego et al., 2003).

The computational and regularization aspects of the non-local model have only been briefly described in this report. Numerical examples presented were used to demonstrate the mesh independence of the obtained solutions. The numerical implementation (Nguyen, 2005; Nguyen and Houlsby, 2008b) of the model used in this study relied on the use of local stiffness matrices. Although use of this local stiffness matrix greatly increases the computational costs, the most time consuming process of the iteration procedure in fact comes from the solution of coupling equations in the stress update routine. The size of this system of coupling equations depends on the number of integration points undergoing damage. This coupling between integration points is due to non-locality and unfortunately unavoidable for this model. Further studies on the computational and regularization aspects of the model are hence required.

From the viewpoint of constitutive modelling, the model used in this study is able to capture essential features of the mechanical behaviour of concrete in tensile regime (e.g. in tension–tension and tension–compression quadrants of 2D principal stress space). Generalization of the mechanism of a single crack, which has been modelled in this study by a simple isotropic damage-plasticity model, has been briefly presented and is expected to progress further in future work. It is also important to consider the capability of the model to capture the material behaviour in mode II fracture as well as in the transition between modes I and II.

Acknowledgements

The authors thank Professor Guy Houlsby (Oxford University) for his advice in the modification of his thermodynamic framework for use in this study. Financial support from the Jenks family (in the USA), provided through the Peter Jenks Vietnam scholarship to the first author while he was working in Oxford, is gratefully acknowledged.

References

Addessi, D., Marfia, S., Sacco, E., 2002. A plastic non-local damage model. Computer Methods in Applied Mechanics and Engineering 191, 1291–1310.
Bazant, Z.P., 1996. Analysis of work-of-fracture method for measuring fracture energy of concrete. ASCE Journal of Engineering Mechanics 122 (2), 138–144.
Bazant, Z.P., 2002. Concrete fracture models: testing and practice. Engineering Fracture Mechanics 69, 165–205.
Bazant, Z.P., Cedolin, L., 1991. Stability of Structures: Elastic, Inelastic, Fracture and Damage Theories. Oxford University press, Oxford, England.
Bazant, Z.P., Oh, B.H., 1983. Crack band theory for fracture of concrete. Materials and Structures (RILEM, Paris) 16, 155–177.

Bazant, Z.P., Pijaudier-Cabot, G., 1989. Measurement of characteristic length of nonlocal continuum. ASCE Journal of Engineering Mechanics 115 (4), 755–767.
Carmeliet, J., 1999. Optimal estimation of gradient damage parameters from localization phenomena in quasi-brittle materials. Mechanics of Cohesive-Frictional Materials 4, 1–16.
Comi, C., 2001. A non-local model with tension and compression damage mechanisms. European Journal of Mechanics A/Solids 20, 1–22.
Crisfield, M.A., 1997. Non-linear Finite Element Analysis of Solids and Structures, vols. 1–2. John Wiley & Sons Ltd..
De Borst, R., Muhlhaus, H-B., 1992. Gradient-dependent plasticity: formulation and algorithmic aspects. International Journal for Numerical Methods in Engineering 35, 521–539.
De Borst, R., Pamin, J., 1996. Gradient plasticity in numerical simulation of concrete cracking. European Journal of Mechanics A/Solids 15 (2), 295–320.
Di Prisco, M., Ferrara, L., Meftah, F., Pamin, J., De Borst, R., Mazars, J., Reynouard, J.M., 2000. Mixed mode fracture in plain and reinforced concrete: some results on benchmark tests. International Journal of Fracture 103, 127–148.
Elices, M., Guinea, G.V., Gomez, J., Planas, J., 2002. The cohesive zone model: advantages, limitations and challenges. Engineering Fracture Mechanics 69, 137–163.
Feenstra, P.H., de Borst, R., 1995. Constitutive model for reinforced concrete. ASCE Journal of Engineering Mechanics 121 (5), 587–595.
Ferrara, L., Di Prisco, M., 2001. Mode I fracture behaviour in concrete: non-local damage modelling. ASCE Journal of Engineering Mechanics 127 (7), 678–692.
Grassl, P., Jirasek, M., 2006. Plastic model with non-local damage applied to concrete. International Journal for Numerical and Analytical Method in Geomechanics 30, 71–90.
Hansen, E., Willam, K., Carol, I., 2001. A two-surface anisotropic damage/plasticity model for plain concrete. In: de Borst, R. (Ed.), Fracture Mechanics of Concrete Materials. A.A. Balkema, Rotterdam, pp. 549–556.
Hatzigeorgiou, G.D., Beskos, D.E., 2002. Static analysis of 3D damaged solids and structures by BEM. Engineering Analysis with Boundary Elements 26 (6), 521–526.
Hordijk, D.A., 1991. Local approach to fatigue of concrete, Ph.D. dissertation, Delft University of Technology, Delft, The Netherlands.
Hordijk, D.A., 1992. Tensile and tensile fatigue behaviour of concrete; experiments, modeling and analyses, Heron, vol. 37, (1), Stevin Laboratory, Delft University of Technology, Delft, The Netherlands.
Houlsby, G.T., Puzrin, A.M., 2000. A thermomechanical framework for constitutive models for rate-independent dissipative materials. International Journal of Plasticity 16, 1017–1047.
Jefferson, A.D., 2003a. Craft – a plastic-damage-contact model for concrete. I. Model theory and thermodynamic considerations. International Journal of Solids and Structures 40, 5973–5999.
Jefferson, A.D., 2003b. Craft – a plastic-damage-contact model for concrete. II. Model implementation with implicit return-mapping algorithm and consistent tangent matrix. International Journal of Solids and Structures 40, 6001–6022.
Jirásek M., 1998, Comparison of non-local models for damage and fracture. LSC Internal report 98/02, Department of Civil Engineering, Swiss Federal Institutive of Technology (EPFL), Lausanne, Switzerland.
Jirásek, M., Patzák, B., 2001, Models for quasibrittle failure: theoretical and computational aspects, ECCM-2001 European Conference on Computational Mechanics, Cracow, Poland, June 26–29.
Jirásek, M., Patzák, B., 2002. Consistent tangent stiffness for nonlocal damage models. Computers and Structures 80, 1279–1293.
Jirásek, M., Rolshoven, S., Grassl, P., 2004. Size effect on fracture energy induced by non-locality. International Journal for Numerical and Analytical Methods in Geomechanics 28, 653–670.
Ju, J.W., 1990. Isotropic and anisotropic damage variables in continuum damage mechanics. Journal of Engineering Mechanics ASCE 116 (12), 2764–2770.
Ladeveze, P., 1983, Sur une theorie de l'endommagement anisotrope, Rapport interne No. 34, LMT Cachan, France.
Le Bellego, C., Dube, J.F., Pijaudier-Cabot, G., Gerard, B., 2003. Calibration of nonlocal damage model from size effect tests. European Journal of Mechanics A/Solids 22, 33–46.
Lee, J., Fenves, G.L., 1998a. A plastic-damage concrete model for earthquake analysis of dams. Earthquake Engineering and Structural Dynamics 27, 937–956.
Lee, J., Fenves, G.L., 1998b. Plastic-damage model for cyclic loading of concrete structures. ASCE Journal of Engineering Mechanics 124 (8), 892–900.
Luccioni, B., Oller, S., Danesi, R., 1996. Coupled plastic-damaged model. Computer Methods in Applied Mechanics and Engineering 129, 81–89.
Mahnken, R., Kuhl, E., 2003. Parameter identification of gradient enhanced damage models with the finite element method. European Journal of Mechanics A/Solids 18, 819–835.
Markeset, G., Hillerborg, A., 1995. Softening of concrete in compression: localization and size effects. Cement and Concrete Research 25 (4), 702–708.
May, I.M., Duan, Y., 1997. A local arc-length procedure for strain softening. Computers and Structures 64 (1–4), 297–303.
Mazars, J., Pijaudier-Cabot, G., 1996. From damage to fracture mechanics and conversely: a combined approach. International Journal of Solids and Structures 33 (20–22), 3327–3342.
Meftah, F., Reynouard, J.M., 1998. A multilayered mixed beam element in gradient plasticity for the analysis of localized failure modes. Mechanics of Cohesive-Frictional Materials 3, 305–322.
Meschke, G., Lackner, R., Mang, H.A., 1998. An anisotropic elastoplastic-damage model for plain concrete. International Journal for Numerical Methods in Engineering 42, 703–727.
Murakami, S., Kamiya, K., 1997. Constitutive and damage evolution equations of elastic-brittle materials based on irreversible thermodynamics. International Journal of Mechanical Science 39 (4), 473–486.
Nguyen, G.D., 2005. A thermodynamic approach to constitutive modelling of concrete using damage mechanics and plasticity theory, D.Phil. dissertation. Department of Engineering Science, University of Oxford, August 2005.
Nguyen, G.D., Houlsby, G.T., 2007. Non-local damage modelling of concrete: a procedure for the determination of parameters. International Journal for Numerical and Analytical Methods in Geomechanics 31, 867–891.
Nguyen, G.D., Houlsby, G.T., 2008a. A coupled damage-plasticity model based on thermodynamic principles: Part I: model formulation and parameter identification. International Journal for Numerical and Analytical Methods in Geomechanics 32 (4), 353–389.
Nguyen, G.D., Houlsby, G.T., 2008b. A coupled damage-plasticity model based on thermodynamic principles: Part II: non-local regularization and numerical implementation. International Journal for Numerical and Analytical Methods in Geomechanics 32 (4), 391–413.
Nguyen, G.D., Korsunsky, A.M., 2006. Damage-plasticity modelling of concrete: calibration of parameters using separation of fracture energy. International Journal of Fracture 139 (2), 325–332.
Ortiz, M., 1985. A constitutive theory for the inelastic behavior of concrete. Mechanics of Materials 4, 67–93.
Perdikaris, P.C., Romeo, A., 1995. Size effect on fracture energy of concrete and stability issues in three-point bending fracture toughness testing. ACI Materials Journal 92 (5), 483–496.
Petersson, P.E., 1981. Crack growth and development of fracture zones in plain concrete and similar materials, Report TVBM-1006, Div. of Build. Mat., Lund Institute of Technology, Lund, Sweden.
Pijaudier-Cabot, G., Bazant, Z.P., 1987. Nonlocal damage theory. ASCE Journal of Engineering Mechanics 113 (10), 1512–1533.
Que, N.S., Tin-loi, F., 2002. An optimization approach for indirect identification of cohesive crack properties. Computers and Structures 80, 1383–1392.
Reinhardt, H., Cornelissen, H.A.W., Hordjil, D.A., 1986. Tensile tests and failure analysis of concrete. ASCE Journal of Structural Engineering 112 (11), 2462–2477.
Rots, J.G., 1988. Computational modelling of concrete fracture. Ph.D. Thesis, Delft University of Technology.
Salari, M.R., Saeb, S., Willam, K.J., Patchet, S.J., Carrasco, R.C., 2004. A coupled elastoplastic damage model for geomaterials. Computer Methods in Applied Mechanics and Engineering 193 (27–29), 2625–2643.

Schreyer, H.L., 2007. Modelling surface orientation and stress at failure of concrete and geological materials. International Journal for Numerical and Analytical Methods in Geomechanics 31 (2), 147–171.
Shi, C., van Dam, A.G., van Mier, J.G.M., Sluys, L.J., 2000. Crack interaction in concrete. In: Wittmann, F.H. (Ed.), Materials for Buildings and Structures EUROMAT, vol. 6. Weinheim, Germany: Wiley-VCH Verlag, pp. 125–131.
Simo, J.C., Ju, J.W., 1987a. Strain- and stress-based continuum damage models. I. Formulation. International Journal of Solids and Structures 23 (7), 821–840.
Simo, J.C., Ju, J.W., 1987b. Strain- and stress-based continuum damage models. II. Computational aspects. International Journal of Solids and Structures 23 (7), 841–869.
Tin-loi, F., Que, N.S., 2001. Parameter identification of quasibrittle materials as a mathematical program with equilibrium constraints. Computer Methods in Applied Mechanics and Engineering 190, 5819–5836.
Yazdani, S., Schreyer, H.L., 1988. An anisotropic damage model with dilatation for concrete. Mechanics of Materials 7 (3), 231–244.
Zhao, J., Sheng, D., Zhou, W., 2005. Shear banding analysis of geomaterials by strain gradient enhanced damage model. International Journal of Solids and Structures 42 (20), 5335–5355.